AVA compliant pre-stack spectral enhancement

Arash JafarGandomi and Henning Hoeber (CGG)*

Summary

Spectral broadening of migrated and stacked seismic images is a commonly used method to enhance the interpretability of reflection data. In this paper we propose a pre-stack AVA compliant spectral broadening approach based on non-stationary wavelet deconvolution. The algorithm employs AVA coupling in the pre-stack domain to broaden the spectra of all traces in each angle gather simultaneously and in an AVA preserving manner. Using synthetic and real data we show that the characteristics of all AVA classes are preserved and that the spectra of all angles are enhanced and better balanced.

Introduction

Data whitening and spectral broadening techniques are routinely applied to migrated seismic images; perhaps even more so with the advent of broadband data, that can be dominated by low frequency energy. Interpreters need white or, even better: blue spectra for optimally resolved seismic reflectivity (Lancaster & Connolly, 2007).

The question then arises how we can apply such spectral broadening methods in a pre-stack manner, without damaging Amplitude Variation with Angle (AVA). One possibility is to apply a deconvolution operator calculated on the stack to all offsets. However, this assumes the wavelet is stable across angles, which in our experience is not necessarily the case. Here we explore a different avenue, where all angles in the pre-stack data are spectrally enhanced simultaneously. In order to preserve AVA we introduce a cost function that couples the data across all angles. Our method uses a linearized sparse AVA inversion approach (e.g., Alemie & Sacchi, 2011). We describe the formulation of the proposed algorithm and test its performance with synthetic and real data.

Methodology

The non-stationary convolutional model (Margrave, 1998) at a given offset or angle in the time-domain may be described as

$$\mathbf{d}_t = \mathbf{W}_t \mathbf{r}_t . \tag{1}$$

Here $\mathbf{d}_t$ and $\mathbf{r}_t$ are the data and reflectivity vectors and $\mathbf{W}_t$ is the time-dependent convolutional wavelet matrix:

$$\mathbf{W}_t = \begin{bmatrix} w_1^1 & & & & & \\ w_2^1 & w_1^2 & & & & \\ w_3^1 & w_2^2 & w_1^3 & & & \\ & w_3^2 & w_2^3 & . & & \\ & & w_3^3 & . & . & w_1^n \\ & & & & . & w_2^n \\ & & & & & w_3^n \end{bmatrix}. \tag{2}$$

The superscript is the time-index of the data and the subscript stands for the wavelet time sample. The time and angle-dependent wavelets may be obtained through statistical wavelet estimation and well-tie. Extending equations 1 and 2 to the pre-stack domain with AVA coupling is achieved by letting:

$$\mathbf{d}_{t,\theta} = \mathbf{W}_{t,\theta}\mathbf{G}_{t,\theta}\mathbf{r}_t , \tag{3}$$

or,

$$\mathbf{d}_{t,\theta} = \mathbf{W}_{t,\theta}\mathbf{r}_{t,\theta} . \tag{4}$$

Here $\mathbf{G}_{t,\theta}$ describes polynomial AVA coupling across offsets or angles. By using this coupling, the algorithm favors events that are present across all angles. Our method starts by solving equation 3 for $\mathbf{r}_t$ using a non-stationary estimate of time- and angle-dependent wavelets $\mathbf{W}_{t,\theta}$ and a sparse inversion algorithm with L1 norm. The estimated $\mathbf{r}_t$ is then converted to $\mathbf{r}_{t,\theta}$ by applying the same AVA coefficients $\mathbf{G}_{t,\theta}$ used to solve Equation 3. Different levels of sparseness may be introduced to enhance the spectral bandwidth of the estimated reflectivity. The inversion proceeds gather by gather, but structural consistency is applied to avoid boosting noise and to improve lateral continuity of $\mathbf{r}_{t,\theta}$ in a dip compliant manner. The structural consistency is applied to the model parameters in 3D through warping (applying time-dependent time-shifts to align adjacent traces) within a moving spatial window and subsequent stacking. The wavelet varies only temporally and we assume zero phase in all examples. The spectrally enhanced data are then formed through:

$$\bar{\mathbf{d}}_{t,\theta} = \overline{\mathbf{W}}_{t,\theta}\mathbf{r}_{t,\theta} , \tag{5}$$

where $\overline{\mathbf{W}}$ is the desired broadband non-stationary wavelet such that

$$Energy\left[\overline{W}_{t,\theta}\right] = Energy\left[W_{t,\theta}\right]. \tag{6}$$

This constraint preserves relative AVA. Neglecting $\mathbf{G}_{t,\theta}$ in Equation 3 leads to an uncoupled deconvolution of multiple traces. It is worth mentioning that even in the uncoupled case the AVA behavior of the input data will be preserved through the energy preserving wavelet scaling, however an additional spectral-angle-balancing may then be required to achieve similar results to the coupled case. The AVA coefficients $\mathbf{G}_{t,\theta}$ in the deconvolution introduce coupling within the multiple traces in a CDP gather that guide the spectral enhancement towards a stationary seismic spectrum in the angle domain. Effects such as residual NMO-stretch and non-stationarity of the seismic wavelet are corrected with this deconvolution approach. Residual Q effects are partially corrected, as the wavelet has no lateral variations. By using an AVA coupled formulation we avoid boosting where data are not AVA consistent across the pre-stack data.

For real data, we must consider a noise term in Equation 4:

$$\mathbf{d}_{t,\theta} = \mathbf{W}_{t,\theta}\mathbf{r}_{t,\theta} + \mathbf{e}_{t,\theta}\,, \tag{7}$$

This noise term is the residual of the inversion. It is possible to add this noise term back to the enhanced data to avoid any potential energy leakage within the original bandwidth of data due to the spectral broadening. Equation 5 is then replaced by:

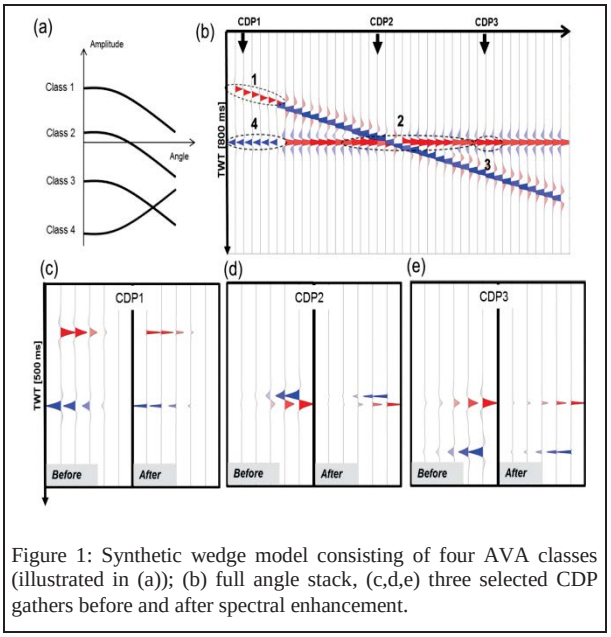

Figure 1: Synthetic wedge model consisting of four AVA classes (illustrated in (a)); (b) full angle stack, (c,d,e) three selected CDP gathers before and after spectral enhancement.

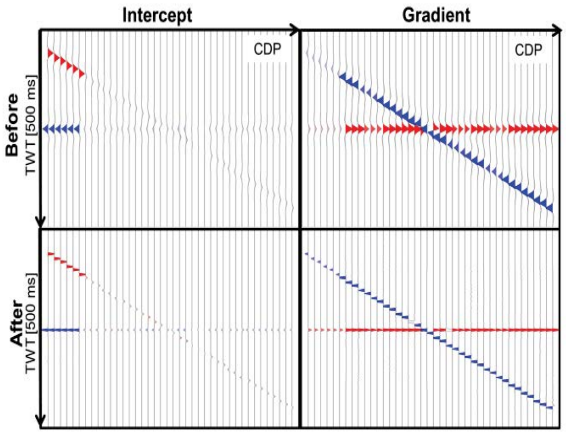

Figure 2: Estimated intercept (left) and gradient (right) from AVA fit before (top) and after (bottom) AVA compliant spectral enhancement.

$$\bar{\mathbf{d}}_{t,\theta} = \overline{\mathbf{W}}_{t,\theta}\mathbf{r}_{t,\theta} + \mathbf{e}_{t,\theta}\,. \tag{8}$$

This can be an effective way to preserve parts of the data, such as vertical faults, that are not fully described by the convolutional model. By adding the noise back, the AVA within the existing bandwidth is naturally preserved and any frequency enhanced part of the spectrum is AVA consistent in the sense of the coupling used.

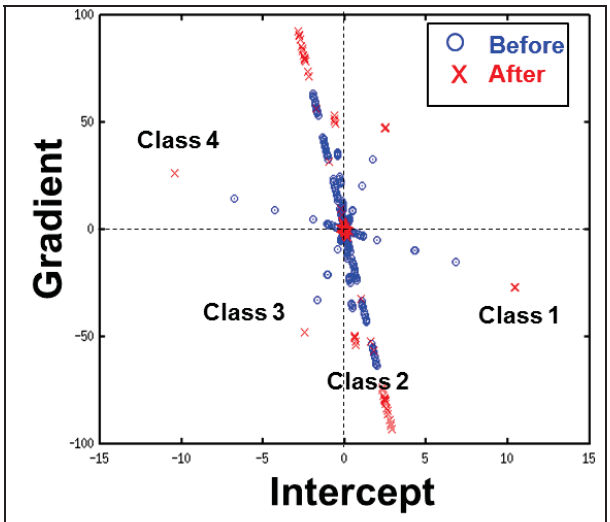

Figure 3: Intercept-gradient cross-plot for the synthetic wedge model of Figure 1 containing four AVA classes. Circles and crosses indicate before and after spectral enhancement, respectively.

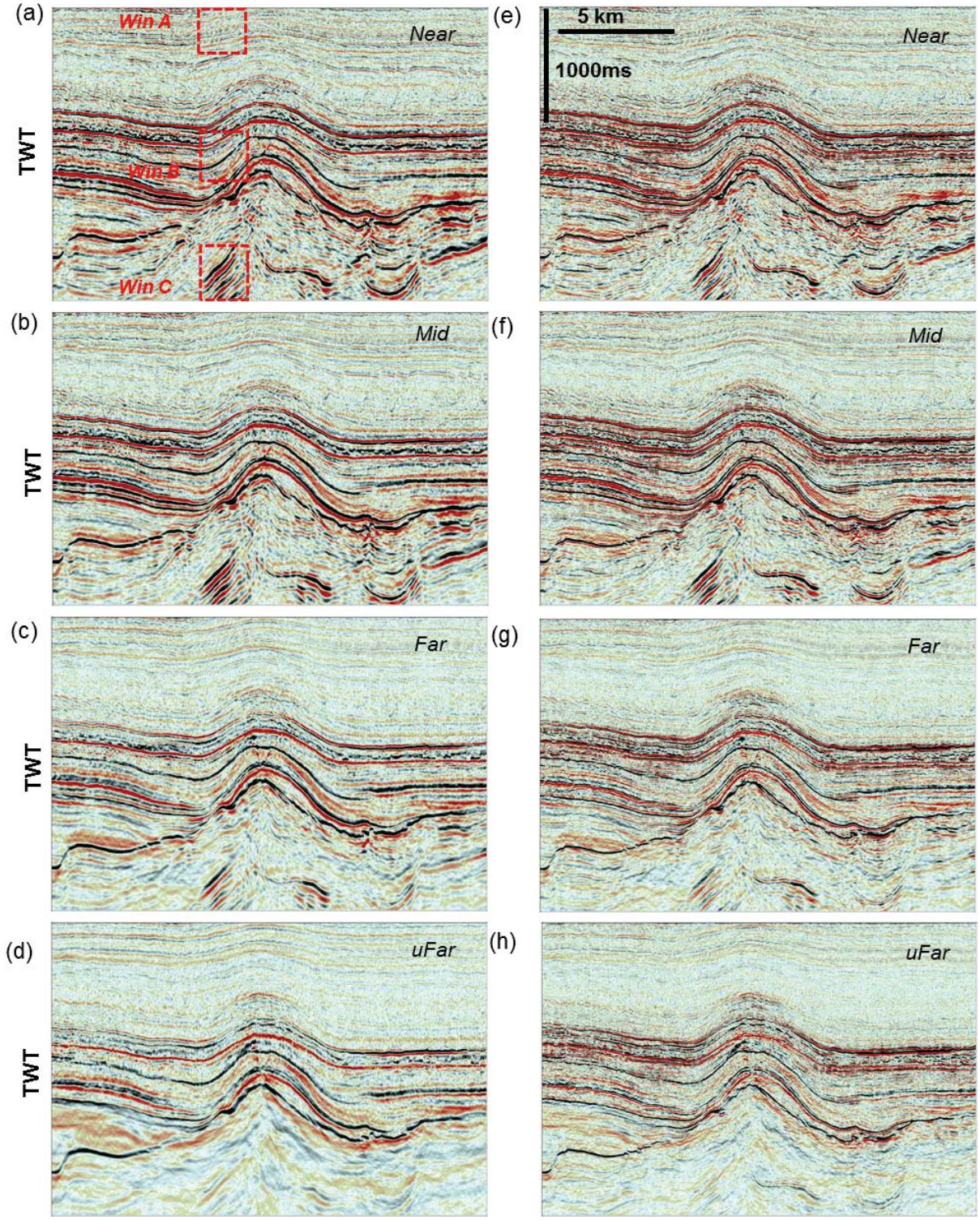

Figure 4: Real data example from the North Sea. (a-d) Input near-, mid- far- and ultrafar-angle stacks, (e-h) corresponding angle-stacks after AVA compliant bandwidth enhancement (Equation 8).

AVA compliant pre-stack spectral enhancement

Synthetic example

We start by examining the performance of the algorithm on a pre-stack synthetic wedge model containing the four major AVA classes (Castagna & Swan, 1997) (Figure 1a). Each synthetic CDP gather contains 5 traces corresponding to 5, 15, 25, 35, and 45 degrees incidence angles. No wavelet differences have been modelled, the only amplitude changes are due to AVA.

Figures 1c, 1d and 1e display CDP gathers before and after spectral enhancement. To verify AVA compliance of the algorithm, an AVA fit is run on the data before and after bandwidth enhancement. Figure 2 shows the estimated intercept and gradient from which we create intercept-gradient cross-plots before and after bandwidth enhancement. Both the intercept and gradient are scaled by the algorithm after enhancement, which is evident in Figures 2 and 3, however no rotation in the intercept-gradient cross-plot is created by the algorithm and relative AVA is clearly preserved for all 4 cases.

Real data example

We now present a North Sea real data example of the proposed algorithm. Prior to application of the algorithm, these data have gone through broadband processing which included source designature/debubble, source and receiver de-ghosting and finally imaged using Kirchhoff pre-stack depth migration. The only absorption compensation applied to the data was a constant phase-only Q-correction before migration. The algorithm was applied to the CDP/angle gathers in the coupled pre-stack mode. The CDP gathers contain 4 traces corresponding to 9, 20, 31, and 39 degrees incidence angles. Figures 4a-d show the near-, mid- , far- and ultrafar-angle stacks before bandwidth enhancement. The corresponding angle stacks after coupled AVA compliant spectral enhancement are shown in Figures 4e-h. These images show that the algorithm has managed to effectively reduce the side lobes and enhance the spectra without boosting noise. The spectra of all angle stacks before and after enhancement are shown in Figure 5a. Despite this algorithm not containing any matching, the AVA cost function leads to better agreeing spectra after the deconvolutions.

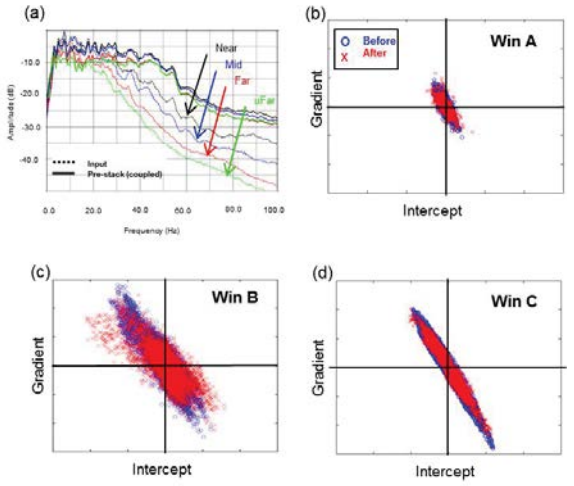

Figure 5: (a) Spectra of near-, mid, far and ufar-angle stacks before (dashed-line) and after (solid line) AVA compliant spectral enhancement. (b-d) Intercept-gradient cross-plot for three selected windows highlighted in Figure 4a.

Finally, we run an AVA fit on the data before and after spectral enhancement. We use three different windows highlighted in red in Figure 4a. The corresponding AVA intercept-gradient cross-plots are presented in Figures 5c-d. We see that the AVA compliant spectral broadening leads to better focused distributions of points in the cross-plot domain. In window B, where there is the potential of an AVA anomaly, we see that the method can lead to better outlier separation from the background trend.

Conclusion

We have presented an AVA compliant pre-stack spectral enhancement method. The algorithm applies non-stationary wavelet de-convolution simultaneously on pre-stack angle-gathers and couples the data with an AVA polynomial. Signal preservation is strengthened by options for 3D structural conformity in the deconvolution operators and by the re-use of the noise model in the existing data bandwidth. The non-stationary wavelet de-convolution gives laterally and temporally more stable wavelets across all angles. We demonstrated the performance of the proposed approach both with a synthetic wedge model and real data. The synthetic model confirms the AVA compliance of the approach through focusing the intercept-gradient cross-plots without rotation of the AVA anomalies. It is also possible to apply the method to stack data; however, running in AVA compliant mode followed by stacking improves the quality of the stack image further whilst avoiding boosting of noise and non AVA compliant signal.

Acknowledgments

We thank the CGG Multi-Clients and New Ventures team for providing us with the real data.

EDITED REFERENCES

Note: This reference list is a copyedited version of the reference list submitted by the author. Reference lists for the 2016 SEG Technical Program Expanded Abstracts have been copyedited so that references provided with the online metadata for each paper will achieve a high degree of linking to cited sources that appear on the Web.

REFERENCES

Alemie, W., and M. D. Sacchi, 2011, High-resolution three-term AVO inversion by means of a Trivariate Cauchy probability distribution: Geophysics, **76**, no. 3, R43–R55, http://dx.doi.org/10.1190/1.3554627.

Castagna, J. P., and H. W. Swan, 1997, Principles of AVO crossplotting: The Leading Edge, **16**, 337–344, http://dx.doi.org/10.1190/1.1437626.

Lancaster, S. J., and P. A. Connolly, 2007, Fractal layering as a model for coloured inversion and blueing: 69th Annual International Conference and Exhibition, EAGE, Extended Abstracts, http://dx.doi.org//10.3997/2214-4609.201401623.

Margrave, G. F., 1998, Theory of nonstationary linear filtering in the Fourier domain with application to time-variant filtering: Geophysics, 63, 244–259, http://dx.doi.org//10.1190/1.1444318.